

# Spring constant modulation in a zone plate tweezer using linear polarization

E. Schonbrun\* and K. B. Crozier

School of Engineering and Applied Science, Harvard University, Cambridge, Massachusetts 02138, USA

\*Corresponding author: schonbru@deas.harvard.edu

Received May 6, 2008; revised July 20, 2008; accepted July 25, 2008;  
posted August 4, 2008 (Doc. ID 95777); published August 29, 2008

At large NAs a micro-Fresnel zone plate produces a focal spot that is more elliptical than that produced by an objective lens with the same NA. Using this anisotropy we demonstrate a method for modulating the spring constant of an optical trap by rotating the linear input polarization. The focal spot ellipticity is enhanced by the apodization factor of the zone plate and its extremely high NA. By measuring the positions of trapped particles we obtain two-dimensional histograms of particle position. These indicate that the trap spring constant is 2.75 times larger perpendicular to the incident polarization than along it. The elliptical focal spot distribution can be rotated by rotating the incident polarization, allowing the spring constant along a given direction to be modulated. © 2008 Optical Society of America  
OCIS codes: 350.4855, 050.1965, 220.1230.

The focusing element is often regarded as the most important component of an optical trap [1]. Tightly trapped particles are strongly influenced by intensity gradients in the focal volume, making trapping performance sensitively dependent on the precise form of the intensity distribution [1,2]. Previously, high-performance optical traps have used microscope objective lenses. Fresnel zone plates, however, can focus light to smaller spots than microscope objectives with the same NA [3]. The resultant larger intensity gradients make them of considerable interest for optical trapping.

In this Letter, we present trapping calibration results for a micro-Fresnel zone plate optical tweezer that has a different apodization function [4] and a significantly larger focusing cone angle than commercial microscope objectives. The zone plate produces an elliptical focal spot distribution that is narrower in the direction perpendicular to the incident polarization than that produced by an aplanatic lens. Calibration of the zone plate optical tweezer shows large trap stiffness relative to focused optical intensity, as well as a spring constant that is a function of the input polarization state. Anisotropic spring constants have been previously observed in objective lenses [5,6], but the ellipticities were smaller, and stiffness modulation was not demonstrated.

We recently demonstrated a micro-Fresnel zone plate optical tweezer fabricated on a microscope slide that was also the primary mechanical mount for the fluidic cell [7]. Several other integrated trapping geometries have been recently demonstrated, including fiber optical traps [8] and parabolic mirror arrays [9]. While the integrated geometries of [8,9] have successfully performed three-dimensional trapping, they have not shown stiffness values that rival conventional systems. Our Fresnel zone plate optical traps have stiffness values comparable to conventional optical tweezers, when the zone plate efficiency is taken into account [7]. In addition, because the zone plate is fabricated on the inner surface of the microfluidic chamber, the distance between the zone plate and

trapped particle is small. This means that the focal length can be exceedingly short, enabling larger focusing cone angles than available with commercial objective lenses. These large angle marginal rays play a crucial role in both tightly focused vector waves and optical trapping.

In addition to the NA, the apodization factor of the focusing element also has a large effect on the field distribution in the focal spot [3,4]. The apodization factor of an aplanatic lens is  $\cos^{1/2} \alpha$  [4], which approaches zero for large angle rays (as  $\alpha$  approaches  $\pi/2$ ). However, the apodization factor for a flat diffractive lens is  $\cos^{-3/2} \alpha$  [3], which diverges for large angle rays. The result is that beams focused by high NA zone plates carry the majority of their energy in the large angular region of their spatial frequency spectrum. Other approaches for increasing the relative energy in large angle rays include using a central field stop [10] or a higher-order Gauss-Laguerre beam [11].

Our Fresnel zone plate consists of 15 concentric gold rings, each 50 nm thick, with the outermost ring having a diameter of 27  $\mu\text{m}$ . For a laser wavelength of 976 nm, electron beam lithography can produce a

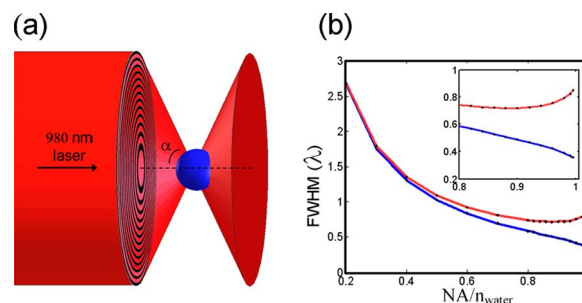


Fig. 1. (Color online) Fresnel zone plate schematic and focal spot size. (a) Illustration of zone plate illumination and maximum focusing angle. (b) FWHM of a zone plate in perpendicular (lower curve) and parallel (upper curve) cross sections through the focus. At small NAs, the focus is circular, and then becomes increasingly elliptical at larger NAs. Inset, expanded plot for NA ranging from 0.8 to 1.0.

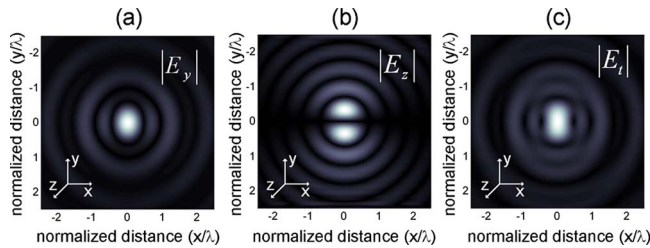


Fig. 2. (Color online) Field distributions of the zone plate focal spot. (a)–(c) show the magnitude of the  $y$ ,  $z$ , and total electric field distributions, respectively. The incident field is polarized in  $y$  and propagates in  $z$ .

zone plate with an NA that is extremely close to its maximum value, the refractive index of water  $n_{\text{water}}$ . With a focal length of  $4\lambda_0/n_{\text{water}}$ , the zone plate has an effective NA of  $0.978 n_{\text{water}}=1.30$ , which means that the maximum focusing cone angle is  $78^\circ$ . By comparison, the cone angle of a water immersion 1.2 NA objective and an oil immersion 1.4 NA objective is  $64^\circ$  and  $68^\circ$ , respectively. Figure 1(a) shows the zone plate and the maximum focusing angle  $\alpha$ .

At large NAs, the FWHM of the focal spot continues to decrease in the cross section perpendicular to the incident polarization toward its limit of approximately  $0.36\lambda_0/n_{\text{water}}$ , as shown in the calculation of Fig. 1(b) (lower curve). Surprisingly, in the cross section parallel to the incident polarization, the width begins to increase at NAs above 0.9, shown in Fig. 1(b) (upper curve). Note that in Fig. 1(b), the NA is normalized to the refractive index of the immersion medium. Using the Debye integral method [4] with the appropriate apodization factor, we analyze the focal spot distributions of the zone plate and an aplanatic lens. With a fill factor of 1.73, the FWHM of the zone plate focal spot is  $0.426\lambda_0/n_{\text{water}}$  by  $0.738\lambda_0/n_{\text{water}}$  in perpendicular and parallel cross sections, respectively. By contrast, for a 1.2 NA water immersion lens with the same fill factor, the FWHM is  $0.537\lambda_0/n_{\text{water}}$  by  $0.719\lambda_0/n_{\text{water}}$ .

A linearly polarized field produces a large axial field component in a high NA focal spot. We used a nonparaxial beam propagation algorithm [12], taking into account vector wave superposition, to simulate the fields produced by the fabricated zone plate. This method accounts for the finite size of the zone plate, unlike the Debye integral approach employed in Fig. 1(b). The transversely polarized field component,

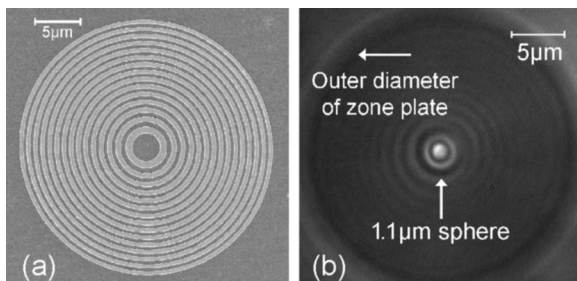


Fig. 3. Fabricated zone plate and the zone plate optical tweezer. (a) Scanning electron micrograph of the gold zone plate. (b) Microscope image of a  $1.1 \mu\text{m}$  latex sphere trapped  $2.9 \mu\text{m}$  ( $=4\lambda_0/n_{\text{water}}$ ) above the substrate.

$E_y$ , shown in Fig. 2(a), maintains a primarily symmetric distribution with a single dominant lobe centered on the optical axis. The spatial distribution of the axial field component,  $E_z$ , is not azimuthally symmetric as shown in Fig. 2(b). It has two main lobes orientated along the polarization direction that increase in amplitude proportional to the sine of the diffracted angle. Because of a zone plate's apodization factor, the amplitude of the axial field component is larger than that of an aplanatic lens, giving the focal distribution a greater ellipticity. We use this unique property of extremely high NA zone plates to implement an optical tweezer that has a large polarization dependent stiffness.

The zone plate optical tweezer, shown as Fig. 3(a), is characterized by tracking the position of a trapped  $1.1 \mu\text{m}$  diameter latex fluorescent sphere. The experimental setup described in [7] is employed. A centroid algorithm is applied to the fluorescence image obtained from a CCD camera, which is shown as Fig. 3(b). By measuring the position of a single dried bead on a microscope slide, we find that the standard deviation of our position measurement is  $2.5 \text{ nm}$ . Figure 4 shows the trapped particle distribution for four different linear polarizations of the incident beam, where  $\theta$  is defined as the angle between the incident polarization and the  $y$  axis. Images are taken at  $30 \text{ Hz}$ , with  $1/64 \text{ s}$  exposure times, for a total of 1000 frames. The centroid position of the bead for each frame is convolved with a Gaussian representing the measurement uncertainty of  $2.5 \text{ nm}$  and plotted.

From the particle position histograms of Fig. 4, the trapping stiffness can be calculated using the equipartition theorem, where the temperature of the water is assumed to be  $25^\circ\text{C}$ . Motion blur from the in-

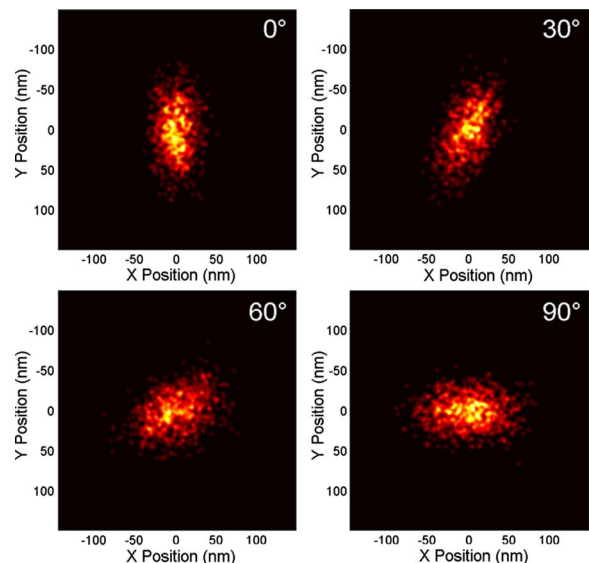


Fig. 4. (Color online) Histograms showing positions of trapped particle at 1000 instants in time. Particle positions are plotted over a  $33 \text{ s}$  duration at  $30 \text{ Hz}$  to map out the trapping potential of the elliptical focus for a laser power of  $40 \text{ mW}$ . Each position is convolved with a Gaussian half-width ( $2.5 \text{ nm}$  half-width) representing measurement uncertainty. The orientation of the incident linear polarization is changed by rotating a half-wave plate.

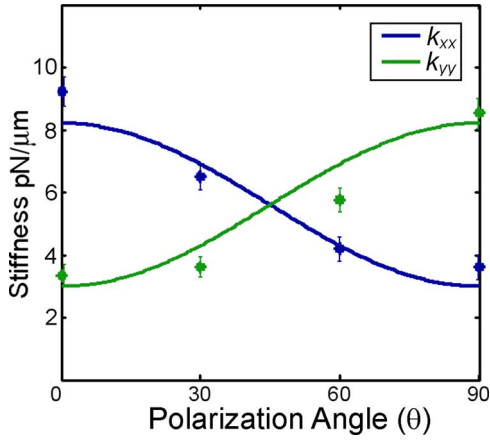


Fig. 5. (Color online) Polarization modulation of the spring constant. The black and gray data points represent the motion blur corrected spring constants  $k_{xx}$  and  $k_{yy}$ , respectively, where the polarization angle is measured with respect to  $\mathbf{y}$ . The solid curves show a least-squares fit obtained with the rotation matrix model.

tegration time of the CCD exposure reduces the measured variance of the distribution, but this is corrected for using the statistics of Brownian motion in a harmonic potential [13]. The orientation of the elliptical trap, described by the forces  $F_x$  and  $F_y$ , rotates along with the polarization angle and is described by

$$\begin{bmatrix} F_x \\ F_y \end{bmatrix} = \begin{bmatrix} k_{xx} & k_{xy} \\ k_{yx} & k_{yy} \end{bmatrix} \begin{bmatrix} x \\ y \end{bmatrix} = \begin{bmatrix} \cos \theta & -\sin \theta \\ \sin \theta & \cos \theta \end{bmatrix} \begin{bmatrix} k_{\text{perp}} & 0 \\ 0 & k_{\text{par}} \end{bmatrix} \times \begin{bmatrix} \cos \theta & \sin \theta \\ -\sin \theta & \cos \theta \end{bmatrix} \begin{bmatrix} x \\ y \end{bmatrix}, \quad (1)$$

where  $k_{xx}$  and  $k_{yy}$  are the spring constants coupling displacement to force along the same direction and  $k_{xy}$  and  $k_{yx}$  couple displacement to force in the orthogonal direction. The spring constant along the polarization is  $k_{\text{par}}$ , perpendicular to the polarization is  $k_{\text{perp}}$ , and  $\theta$  is the polarization angle relative to  $\mathbf{y}$ . By measuring the variance along  $\mathbf{x}$  and  $\mathbf{y}$  and using the equipartition theorem [1], we can evaluate  $k_{xx}$  and  $k_{yy}$  as a function of  $\theta$ . Fitting the data to Eq. (1), we find that  $k_{\text{perp}}$  has a stiffness of 8.21 pN/ $\mu\text{m}$  and  $k_{\text{par}}$  has a stiffness of 2.98 pN/ $\mu\text{m}$  for a laser power of 40 mW. The diffracted power in the focal spot is estimated to be 2 mW owing to the zone plate diffraction efficiency ( $1/\pi^2$ ) and overfilling of the back aperture. Using these values for  $k_{\text{perp}}$  and  $k_{\text{par}}$ , the spring constant tensor  $k$  can be evaluated for any angle  $\theta$ .

Figure 5 shows both the experimental data and the results of fitting to the rotation matrix model. By

changing the incident polarization, the stiffness of the trap can be modulated by a factor of 2.75 without changing the incident power or location of the trap center. Uncertainty in the variance owing to a finite number of measurements produces the error bars shown in Fig. 5. There is some asymmetry between  $k_{xx}$  and  $k_{yy}$ , with the maximum value of  $k_{yy}$  being smaller. This is consistent with our observation of convection currents in  $\mathbf{y}$ , which arise from the heating of the gold and, consequently, the water. Heating of the water also adds uncertainty to force calibration owing to temperature fluctuations. The magnitude by which the force can be modulated using linear polarization rotation is a function of the difference between  $k_{\text{perp}}$  and  $k_{\text{par}}$ . This anisotropy is enhanced by the focal spot ellipticity, but it is also a function of sphere size [6].

The focal spot distribution at large NAs is sensitively dependent on the incident polarization. This sensitivity arises from the axially polarized field component that is dominant in the marginal rays focused by the optical element. A Fresnel zone plate is ideally suited for this application because of the prominence of marginal rays owing to its apodization factor and because large NAs can be implemented in a practical fashion. By taking advantage of the ellipticity of the focus, we present a method for modulating the spring constant of an optical tweezer by rotating the incident linear polarization. The ability to control optical field distributions with diffractive optics and other nanostructures will continue to add functionality to particle manipulation and measurement.

## References

1. K. C. Neuman and S. M. Block, *Rev. Sci. Instrum.* **75**, 2787 (2004).
2. A. Ashkin, J. M. Dziejic, J. E. Bjorkholm, and S. Chu, *Opt. Lett.* **11**, 288 (1986).
3. N. Davidson and N. Bokor, *Opt. Lett.* **29**, 1318 (2004).
4. B. Richards and E. Wolf, *Proc. R. Soc. London, Ser. A* **253**, 358 (1959).
5. W. H. Wright, G. J. Sonek, and M. W. Burns, *Appl. Opt.* **33**, 1735 (1994).
6. A. Rohrbach, *Phys. Rev. Lett.* **95**, 168102 (2005).
7. E. Schonbrun, C. Rinzler, and K. B. Crozier, *Appl. Phys. Lett.* **92**, 071112 (2008).
8. A. Constable, J. Kim, J. Mervis, F. Zarinetchi, and M. Prentiss, *Opt. Lett.* **18**, 1867 (1993).
9. F. Merenda, J. Rohner, J. Fournier, and R. Salathe, *Opt. Express* **15**, 6075 (2007).
10. R. Gussgard, T. Lindmo, and I. Brevik, *J. Opt. Soc. Am. B* **9**, 1922 (1992).
11. N. B. Simpson, D. McGloin, K. Dholakia, L. Allen, and M. J. Padgett, *J. Mod. Opt.* **45**, 1943 (1998).
12. J. E. Harvey, *Am. J. Phys.* **47**, 974 (1979).
13. W. P. Wong and K. Halvorsen, *Opt. Express* **14**, 12517 (2006).